CONTINUOUS STRUCTURAL MONITORING OF AGING AIRCRAFT WITHOUT USING REFERENCE DATA

Hoon Sohn, Ph.D.

Associate Professor

Civil and Environmental Engineering Department

Korea Advanced Institute of Science and Technology

Funding Agency: Asian Office of Aerospace Research and Development, Department of the Air Force, US

Funding Period: June 01, 2007 to May 31, 2009

Funding level: $50,000 for two years

ABSTRACT

The goal of this proposal is to develop a new NDT concept and theory based on Lamb waves, in which damage can be detected "without relying on past reference data." In particular, a NDT methodology will be formulated for detecting defects such as crack, corrosion and delamination commonly found in aircraft. To the PI's best knowledge, no other group or literature has addressed NDT issues from this new viewpoint. The proposed concept of "reference-free" damage diagnosis attempts to address some of the fundamental technical hurdles that have to be overcome before NDT systems can be deployed for continuous monitoring of aircraft. The intent of the present approach is not to disregard useful prior knowledge or information gained but to relax explicit dependency on baseline data so that the proposed methodology can be made more attractive for aircraft monitoring during its normal operation. By incorporating the proposed approach to the conventional NDT techniques, it is envisioned that more reliable damage diagnosis can be achieved.

First, the theoretical framework for the proposed reference-free diagnosis will be developed based on the polarization characteristics of lead zirconate titanate (PZT) wafer transducers. Then, features that are sensitive to damage but insensitive to ambient variations of aircraft in the field will be extracted by comparing two instantaneous collected signals without referencing to past baseline data. Here, active sensing devices such as lead zirconate titanate will be used to generate and measure guided waves in metallic structures. Once damage-sensitive features are identified, statistical classifiers will be developed to establish decision boundaries without using prior reference data and to minimize false indications of damage. Finally, realistic environmental and operational conditions that in-service aircraft is subject to will be explicitly considered.

This strategy offers a potential for a significant breakthrough in SHM/NDT practice via the integration of active sensing, smart materials, statistical pattern recognition techniques and new theoretical development for damage diagnosis that has not been attempted to date. To the primary investigator's best knowledge, no other group or literature has addressed NDT from this point of view: "baseline-free" damage diagnosis. This field deployable NDT technique will be unique because (1) damage diagnosis can be accomplished without relying on prior reference data, (3) the monitoring system will have its own "intelligence" that autonomously converts real-time sensor data to damage diagnosis information without requiring data interpretation by the end users, (4) the proposed NDT paradigm can be applied to complex geometries such as welded/bolted connections where defects often occur, and (5)

Report Documentation Page

Form Approved
OMB No. 0704-0188

1. REPORT DATE	2. REPORT TYPE	3. DATES COVERED
28 JAN 2010	**FInal**	**04-04-2007 to 01-04-2009**

4. TITLE AND SUBTITLE
Continuous Structural Monitoring of Aging Aircraft without using reference data

5a. CONTRACT NUMBER
FA48690714054

5b. GRANT NUMBER

5c. PROGRAM ELEMENT NUMBER

6. AUTHOR(S)
Hoon Sohn

5d. PROJECT NUMBER

5e. TASK NUMBER

5f. WORK UNIT NUMBER

7. PERFORMING ORGANIZATION NAME(S) AND ADDRESS(ES)
Korean Advanced Institute of Science and Technology,373-1 Guseong-Dong,Daejeon 305-01,Korea (South),KR,305-01

8. PERFORMING ORGANIZATION REPORT NUMBER
N/A

9. SPONSORING/MONITORING AGENCY NAME(S) AND ADDRESS(ES)
AOARD, UNIT 45002, APO, AP, 96337-5002

10. SPONSOR/MONITOR'S ACRONYM(S)
AOARD

11. SPONSOR/MONITOR'S REPORT NUMBER(S)
AOARD-074054

12. DISTRIBUTION/AVAILABILITY STATEMENT
Approved for public release; distribution unlimited

13. SUPPLEMENTARY NOTES

14. ABSTRACT

The goal of this proposal is to develop a new NDT concept and theory based on Lamb waves, in which damage can be detected ?without relying on past reference data.? In particular, a NDT methodology will be formulated for detecting defects such as crack, corrosion and delamination commonly found in aircraft. To the PI?s best knowledge, no other group or literature has addressed NDT issues from this new viewpoint. The proposed concept of ?reference-free? damage diagnosis attempts to address some of the fundamental technical hurdles that have to be overcome before NDT systems can be deployed for continuous monitoring of aircraft. The intent of the present approach is not to disregard useful prior knowledge or information gained but to relax explicit dependency on baseline data so that the proposed methodology can be made more attractive for aircraft monitoring during its normal operation. By incorporating the proposed approach to the conventional NDT techniques, it is envisioned that more reliable damage diagnosis can be achieved.

15. SUBJECT TERMS
Aging Aircraft, Non-destructive Evaluation, reference-free prognosis

16. SECURITY CLASSIFICATION OF:			17. LIMITATION OF ABSTRACT	18. NUMBER OF PAGES	19a. NAME OF RESPONSIBLE PERSON
a. REPORT	b. ABSTRACT	c. THIS PAGE			
unclassified	**unclassified**	**unclassified**	**Same as Report (SAR)**	**25**	

environmental and operational variations that in-service structures experience will not affect damage diagnosis, minimizing false indications of damage.

1. Introduction

The goal of this proposal is to develop a new NDT concept and theory based on Lamb waves, in which damage can be detected "without relying on past reference data." In particular, a NDT methodology will be formulated for detecting defects such as crack, corrosion and delamination commonly found in aircraft. To the PI's best knowledge, no other group or literature has addressed NDT issues from this new viewpoint. The proposed concept of "reference-free" damage diagnosis attempts to address some of the fundamental technical hurdles that have to be overcome before NDT systems can be deployed for continuous monitoring of aircraft. The intent of the present approach is not to disregard useful prior knowledge or information gained but to relax explicit dependency on baseline data so that the proposed methodology can be made more attractive for aircraft monitoring during its normal operation. By incorporating the proposed approach to the conventional NDT techniques, it is envisioned that more reliable damage diagnosis can be achieved. Specific objectives of the project are:

- **Task 1: Understanding Time Reversibility and PZT Polarization Characteristics:** This study will explore the PZT polarization characteristics and time reversal acoustics for online monitoring of defects in aircraft structures. In this task, theoretical, numerical and experimental investigations will be conducted to better understand the time reversibility of Lamb waves and the polarization characteristics of lead zirconate titanate (PZT) wafer transducers.
- **Task 2: Extraction of Reference-Free Features:** Based on the advanced understanding of time reversibility of Lamb waves and PZT polarization characteristics, this task will explore the PZT polarization characteristics and time reversal process to extract baseline-free features that are sensitive to defects but insensitive to operational and environmental variations of aircraft.
- **Task 3: Instantaneous Damage Diagnosis:** Once damage-sensitive features are identified, a theoretical framework for statistical damage diagnosis will be developed to fully automate the decision-making procedure. Special attention will be paid to instantaneously determine decision boundaries for damage diagnosis without relying on previously established thresholds and to minimize false alarms of damage.
- **Task 4: Environmental and Operational Variations:** Realistic environmental and operational conditions, such as temperature changes and ambient loading, that in-service aircraft is subject to, will be explicitly taken into consideration through laboratory specimen tests and flight tests of aircraft. In addition, practical instrumentation issues such as variations in PZT transducer size, bonding condition and alignment will be investigated.
- **Task 5: Extension to More Complex Structures:** Once the basic concept of the reference-free NDT technique is established, this concept will be extended for more complex components found in aircraft. For instance, this task will investigate the effects of stringers, holes, and bolts in composite lap joints, on the proposed approach.

2. Theoretical Background

The development of the new NDT technique proposed in this project was based on the use of PZT wafer transducers and Lamb waves propagating along thin plate structures. In this part of the report, the effect of PZT poling direction on Lamb wave propagation is discussed first. Then, the damage detection procedure using instantaneously measured Lamb wave signals is introduced briefly.

2.1 The effect of PZT poling directionality on Lamb wave propagation

In this section, it is investigated how the phase of a Lamb wave mode changes depending on (1) the poling directions of exciting and sensing PZT wafer transducers and (2) whether a wafer transducer is attached either on the top or bottom surface of a plate. For illustration, it is assumed four identical PZT wafer transducers, labeled as "A", "B",

"C", and "D", are attached to a plate as shown in Figure 1 (a). The arrows indicate positive poling directions of PZT transducers. PZTs A and D are placed exactly at the same position but on the other side of the plate. PZTs B and C are positioned in a similar fashion. Furthermore, it is assumed that a narrowband toneburst signal is applied as an input, and the driving frequency is chosen such that only the fundamental symmetric (S_0) and anti-symmetric (A_0) modes are generated. In this paper, the term of "positive bending" is used when the positively polarized side of the PZT is subjected to tensile strain. On the other hand, the PZT is subjected to negative bending when the negatively polarized side of the PZT is subjected to tensile strain. The positive bending produces a "positive" output voltage while the negative bending results in a "negative" output voltage value.

When PZT A is excited, the S_0 and A_0 modes are generated and measured at PZTs B and C [1]. In an ideal condition, the amplitude and arrival time of the S_0 modes measured at PZTs B and C should be identical. In addition, both PZTs B and C would be subjected to positive bending because of the symmetric nature of the S_0 mode. Because both PZTs B and C are subject to the positive bending, the phase as well as the amplitude and arrival time of the S_0 mode measured at these PZTs is identical. As far as the A_0 mode is concerned, PZT C is subjected to the negative bending although PZT B still undergoes the positive bending. Therefore, the A_0 modes measured at PZTs B and C are out-of-phase. However, when the poling direction of PZT C is switched [Figure 2 (a)], PZTs B and C will produce out-of-phase S_0 modes and in-phase A_0 modes [Figure 2 (b) and Figure 3 (b)].

In the following section, the effect of PZT poling directionality is further investigated so that the mode conversion due to crack formation can be extracted from the measured Lamb wave signals.

(a) Test configuration I with collocated PZTs with the opposite poling directions

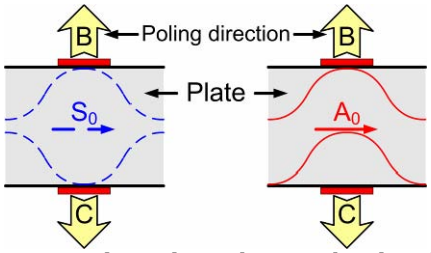

(b) The S_0 mode produces the same bending for PZTs B and C while the A_0 mode results in the opposite bending.

Figure 1. The effect of the PZT poling directions on the phases of the S_0 and A_0 modes (Configuration I)

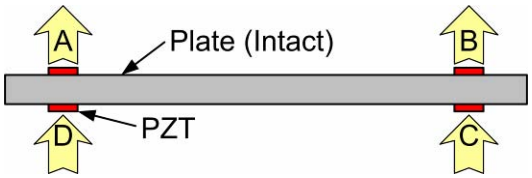

(a) Test configuration II with all PZTs with the same poling directions

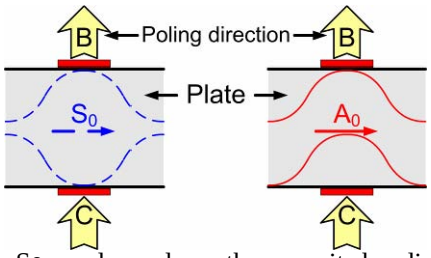

(b) The S_0 mode produces the opposite bending for PZTs B and C while the A_0 mode results in the same bending.

Figure 2. The effect of the PZT poling directions on the phases of the S_0 and A_0 modes (Configuration II)

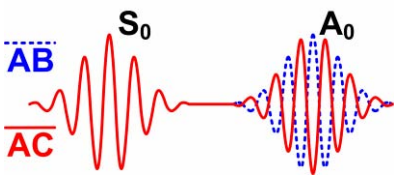

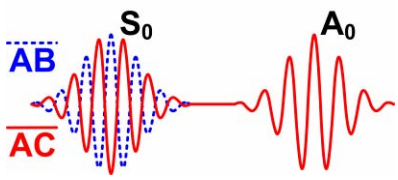

(a) S_0 and A_0 modes measured from configuration I in Figure 1 (a): S_0 modes in-phase & A_0 modes out-of-phase

(b) S_0 and A_0 modes measured from configuration II in Figure 2 (a): S_0 modes out-of-phase & A_0 modes in-phase

Figure 3. A schematic comparison of the S_0 and A_0 modes measured from Configurations I and II shown in Figure 1 (a) and Figure 2 (a), respectively: AB (a dash line) and AC (a solid line) denote the response signals measured at PZTs B and C when a toneburst input is applied at PZT A.

2.2. Detection of crack induced mode conversion using a PZT poling direction

In this section, the PZT polarization characteristic is further advanced so that the mode conversion due to crack formation can be detected without using any prior baseline data. First, the effect of a crack on Lamb wave modes is described. If Lamb waves propagating along a thin plate with a uniform thickness encounter a discontinuity such as a sudden thickness variation of the plate, some portion of the waves are reflected at the discontinuity point and others are transmitted through it. When a S_0 mode arrives at the discontinuity as shown in Figure 4, the transmitted wave is separated into S_0 and A_0 modes (denoted as S_0/S_0 and A_0/S_0, respectively). In a similar manner, an A_0 mode is also divided into S_0 and A_0 modes (S_0/A_0, and A_0/A_0). Similarly, the reflected waves are split to S_0 and A_0 modes. This phenomenon is called mode conversion [2].

In order to fully investigate the sign changes of Lamb wave modes due to mode conversion, sign notations are defined first. In Figure 5, sign notations for the S_0 and A_0 modes are defined schematically. As shown in Figure 5 (a), the S_0 and A_0 modes are defined to be positive when they cause the deformed shape of the specimen's top surface to be convex. On the other hand, the S_0 and A_0 modes are called negative when the deformed shape of the top surface becomes concave [Figure 5 (b)]. In Figure 6, it is shown how the signs of Lamb wave modes are determined as they transmit through a crack. From numerical simulations and experiments, it has been shown that the sign of a single (non-converted) mode is not affected by crack formation. That is, a positive S_0 mode always produces a positive S_0/S_0 mode, and a negative A_0 mode generates a negative A_0/A_0 mode, respectively.

On the other hand, the signs of newly generated modes (A_0/S_0 and S_0/A_0) can be altered depending on the characteristics of a discontinuity that the launching Lamb mode is passing through. Although the signs of these converted modes cannot be determined without knowing the detailed characteristics of the discontinuity, certain relationships among these converted modes can be revealed. For instance, if a positive S_0 mode creates a positive A_0/S_0 mode, a positive A_0 mode also produces a positive S_0/A_0 mode. That is, the signs of the A_0/S_0 and S_0/A_0 modes should be always identical. This is based on the reciprocity of signals AB and BA [3]. Here, signal AB denotes the response signal measured at PZT B when the excitation is applied at PZT A. In order for signals AB and BA to be identical, the shape, amplitude and phase of the A_0/S_0 mode in signal AB should be identical to those of the S_0/A_0 mode in signal BA. In addition, the sign of the A_0/S_0 mode created from a positive S_0 mode should be always opposite to that of the A_0/S_0 mode generated from a negative S_0 mode.

In Figure 7 (a) and Figure 7 (b), the phases of the S_0 and A_0 modes in signals AB and CD are compared when the specimen is in an intact condition. As for signal AB, when PZT A generates positive S_0 and A_0 modes, both modes produce positive bending in PZT B as shown in the upper part of Figure 7(a). On the other hand, PZT C in signal CD creates a negative S_0 mode and a positive A_0 mode because the poling direction of PZT C is opposite to PZT A as shown in the lower part of Figure 7 (a). However, because the poling directions of PZT B and D are also opposite each other, the negative S_0 mode will produce positive bending in PZT B and the positive A_0 mode produces positive bending as well. As a consequence, the phases of the S_0 and A_0 modes measured at PZT D are always identical to those measured at PZT B. Therefore, when the plate is in a pristine condition and four identical PZTs are instrumented as shown in Figure 7 (a), it is concluded that signal AB becomes identical to signal CD as shown in Figure 7 (b).

However, signal AB is no longer identical to signal CD when there is a crack between PZTs A and B (or PZTs C and D) as shown in Figure 7 (c) and Figure 7 (d). As for signal AB, the S_0/A_0 mode arrives at PZT B earlier than the A_0/S_0 mode when the notch is located closer to PZT A than PZT B (assuming that the S_0 mode travels faster than the A_0 mode). Therefore, the S_0 mode is followed by the S_0/A_0, A_0/S_0, and A_0 modes in signal AB. Based on the sign convention in Figure 6, both the S_0/A_0 and A_0/S_0 modes are positive so that the signs of all modes are the same in signal AB. On the other hand, the S_0 mode is followed by A_0/S_0, S_0/A_0, and A_0 modes in signal CD because the S_0/A_0 mode arrives at PZT D later than the A_0/S_0 mode. In this case, a negative A_0/S_0 mode and a positive S_0/A_0 mode are created because of a negative S_0 mode and a positive A_0 mode, respectively [Figure 6]. Note that signal CD has two S_0 modes, S_0/A_0 and S_0, and their signs are opposite. Also, two A_0 modes in signal CD, A_0/S_0 and A_0, have opposite signs as well.

In Figure 7 (d), signals AB and CD are drawn considering not only the arrival times of each modes but also their relative signs (or phases). Note that, while the S_0 and A_0 modes in Figure 7 (d) are in-phase, the S_0/A_0 and A_0/S_0 modes in signals AB and CD are fully out-of-phase. Therefore, the additional modes generated by a notch can be extracted simply by subtracting signal AB from signal CD as shown in Figure 7 (d). In addition to signals AB and CD, it can be readily shown that the S_0 and A_0 modes in signals AC and BD are identical while the S_0/A_0 and A_0/S_0 modes are fully out-of-phase. Because this approach relies only on the comparison of two instantaneous signals obtained at the current state of the system rather than comparison with previously recorded reference data, it is expected that this approach may reduce false alarms of defects due to changing operational and environmental conditions of the system.

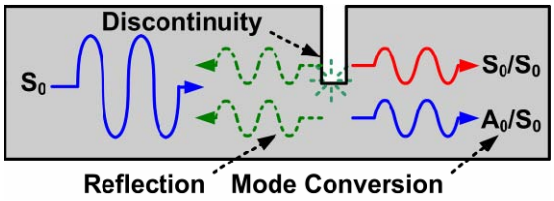

Figure 4. A schematic diagram of mode conversion and reflection due to a discontinuity on a plate

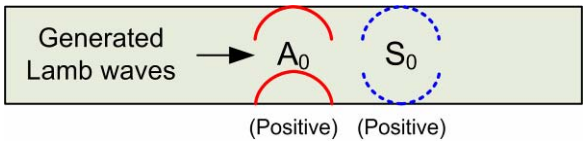

(a) Positive S_0 and A_0 modes (The top surface of the specimen becomes convex)

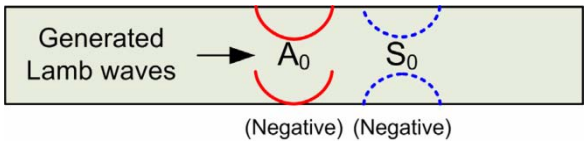

(b) Negative S_0 and A_0 modes (The top surface of the specimen becomes concave)

Figure 5. Sign definitions of the S_0 and A_0 modes traveling in a plate specimen

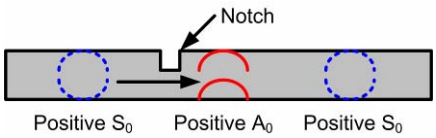

(a) Mode conversion of a positive S_0 mode

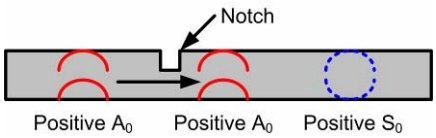

(b) Mode conversion of a positive A_0 mode

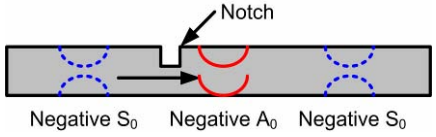

(c) Mode conversion of a negative S_0 mode

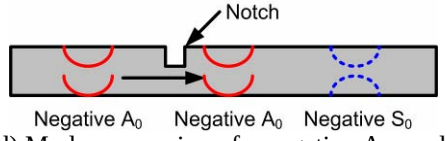

(d) Mode conversion of a negative A_0 mode

Figure 6. Relative phase information of the S_0 and A_0 modes during the mode conversion process due to crack formation

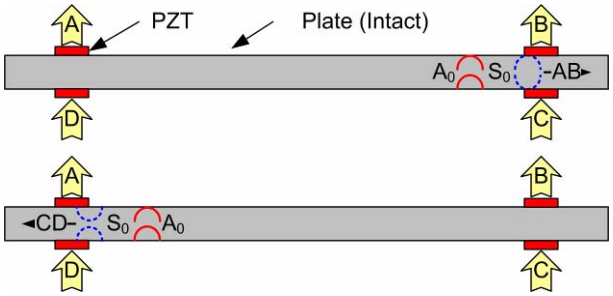

(a) An intact plate with the PZT configuration II shown in Figure 2 (a)

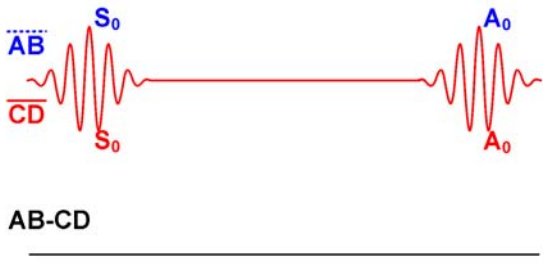

(b) Comparison of signals AB and CD without a notch: the S_0 & A_0 modes are identical

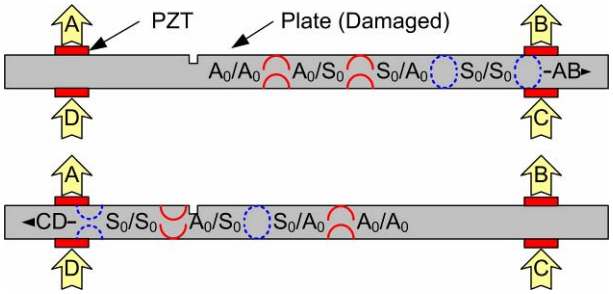

(c) A damaged plate with the PZT configuration II shown in Figure 2 (a)

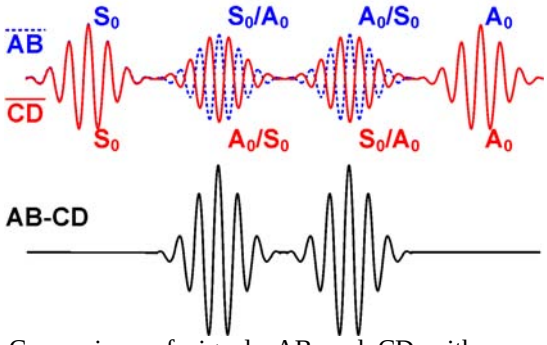

(d) Comparison of signals AB and CD with a notch: the S_0 & A_0 modes are identical, but the S_0/A_0& A_0/S_0 modes are out-of-phase

Figure 7. Extraction of the additional Lamb wave modes generated by a notch by comparing signals AB and CD (A_0/S_0 mode denotes an A_0 mode converted from a S_0 mode when it passes through a crack. S_0/A_0 is defined similarly).

3. Project Activities

3.1. Extraction of reference-free features

In the beginning of the project, the idea of extracting converted Lamb wave modes due to damage using strategically placed PZT transducers was validated first. For the verification, not only numerical simulation but also experiment was conducted.

3.1.1. Numerical simulation

Using COMSOL 3.3a Multiphysics software (www.comsol.com), Lamb wave propagation in a two dimensional aluminum plate was simulated using the combination of plain strain, piezo plain strain, and electrostatics modules in COMSOL software. The length of the plate was 70cm, and its thickness was 6 mm. Four identical PZTs with 10 mm length and 0.508 thickness were attached to the plate model as shown in Figure 8. Note that PZTs A and D were collocated but on the other side of the plate with the same poling direction. PZTs B and C were placed in a similar fashion. The parameter values used in the numerical simulation are listed in Table 1.

Figure 9 (a) illustrates that signals AB and CD were almost identical and this well matches with the theory. Once a notch of 3 mm depth and 1 mm width was introduced 100 mm away from PZT A toward PZT B, signal AB became different from signal CD as a result of the mode conversion induced by the crack as

illustrated in Figure 9 (b). In the following experimental results, the outcome of this numerical simulation is further substantiated.

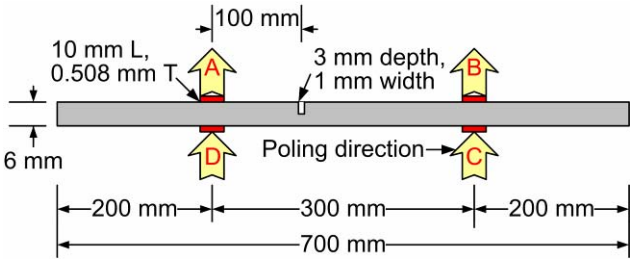

Figure 8. Dimension of an aluminum plate used in numerical simulation

Table 1. Parameters used in numerical simulation

Parameters	Values
Exciting frequency	150 kHz
α (Mass damping coefficient)	10^{-4}
β (Stiffness damping coefficient)	0
Sampling rate	4 MS/s
Relative tolerance	10^{-4}
Absolute tolerance	10^{-10}
Maximum BDF order	2
Mesh size (Mapped mesh)	1 mm x 1 mm maximum

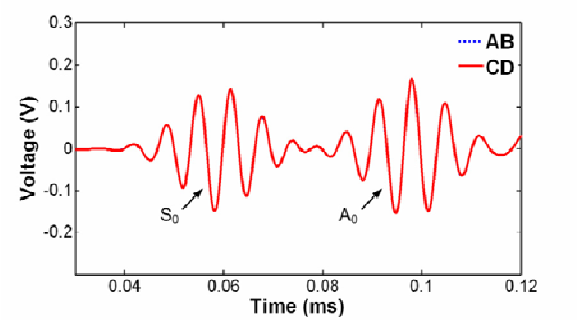

(a) Signals AB and CD without a notch

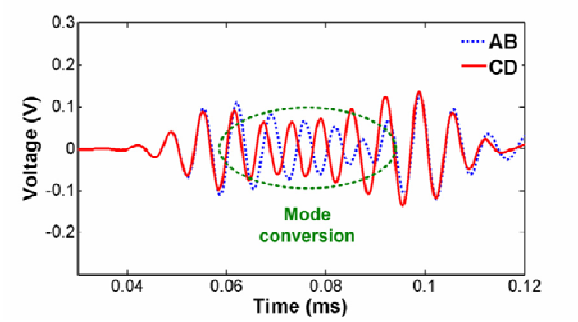

(b) Signals AB and CD with a notch

Figure 9. Comparison of signals AB and CD (or signals AC and BD) when there is no notch Comparison of signals AB and CD (or signals AC and BD) with a notch of 3 mm depth and 1 mm width

3.1.2. Experimental results

To further examine the proposed reference-free NDT technique, experimental tests have been conducted on an aluminum plate. The overall test configuration and the test specimen are shown in Figure 10. The data acquisition system was composed of an arbitrary waveform generator (AWG), a high-speed signal digitizer (DIG), a low noise preamplifier (LNP) and a multiplexer. The dimension of the plate was 122 cm x 122 cm x 0.6 cm, and four PSI-5A4E type PZT wafer transducers (1.0 cm x 1.0 cm x 0.0508 cm) were mounted in the middle of the plate. PZTs A and D were collocated and attached on the other side of the plate, and PZTs B and C were mounted in a similar fashion. The PZTs were attached so that their poling directions were identical to the configuration shown in Figure 2 (a). PZTs A and B (or PZTs C and D) were 0.52 m apart each other. In this experiment, the PZT transducers were attached to either the top or the bottom surface of the plate with commercial cyanoacrylate adhesive.

Using the 14-bit AWG, a toneburst signal with a 10 peak-to-peak voltage and a driving frequency of 150

kHz was generated and applied. First, PZT A in Figure 10 (b) was excited by this input waveform. Then, PZT A generated elastic waves and the response was measured at PZT B. When the waves arrived at PZT B, the voltage output from PZT B was amplified by the LNP with a gain of twenty and measured by the DIG. The sampling rate and resolution of the DIG were 20 MS/sec and 16 bits, respectively. In order to improve the signal-to-noise ratio, the forwarding signals were measured twenty times and averaged in the time domain. After the forwarding signals from PZT A to PZT B (signal AB) were measured, the same process was repeated by measuring signals AC, BD and CD. The entire experimental process without averaging took less than 10 seconds.

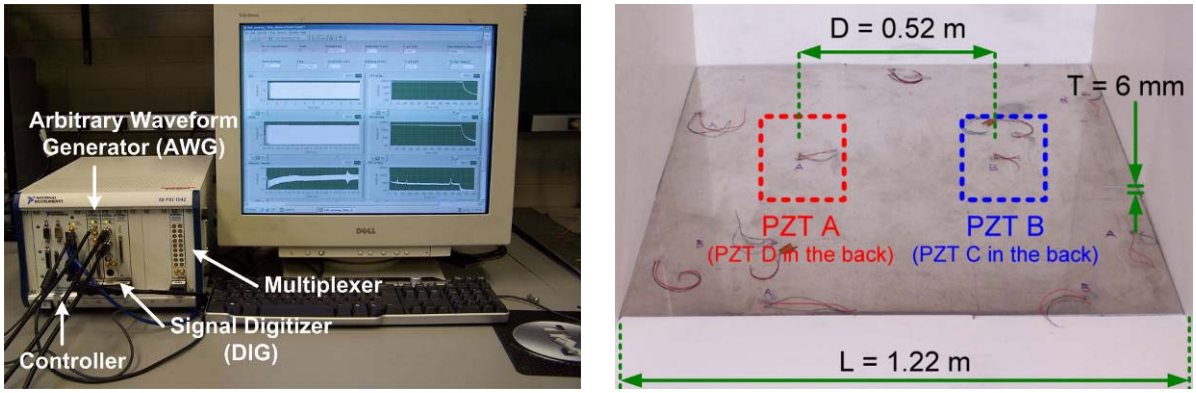

(a) A data acquisition system (b) A square aluminum plate

Figure 10. Testing configuration for detecting a crack on an aluminum plate

In Figure 11, signals AB and CD is instantaneously measured from the pristine condition of the specimen and shown. Figure 11 (b) shows an initial difference between signals AB and CD even in the absence of a crack due to imperfections in PZT alignment, size and bonding condition. Next, a 3 mm (depth) x 1 mm (width) x 60 mm (length) notch was introduced between PZTs A and B (or PZTs C and D). The notch was located 150mm away from PZT A toward PZT B. As a consequence, two additional modes due to mode conversion appeared between the existing S_0 and A_0 modes as shown in Figure 12 (a). Comparison of Figure 11(b) and Figure 12(b) clearly demonstrates the appearance of the additional modes due to crack formation.

However, it is not clear in practice how large the signal difference should be before it leads to warning of damage. To tackle this issue, a new instantaneous damage diagnosis technique is proposed in section 3.2.

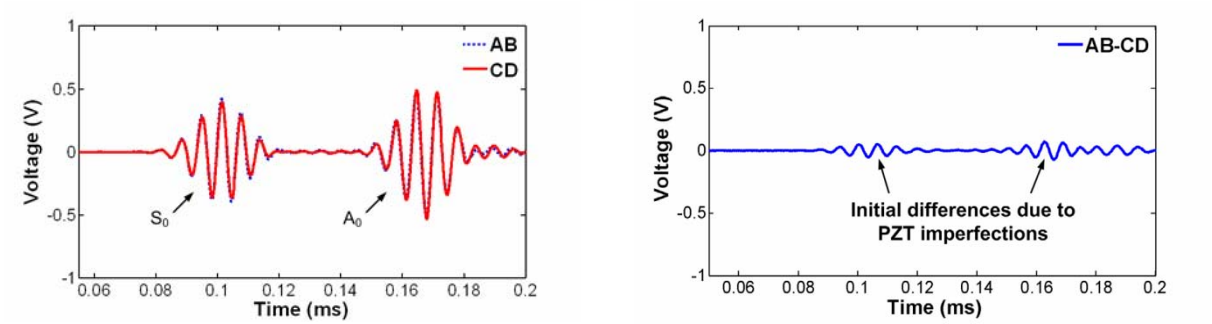

(a) Signals AB and CD without notch (b) Difference between signals AB and CD

Figure 11. Comparison of signals AB and CD without notch

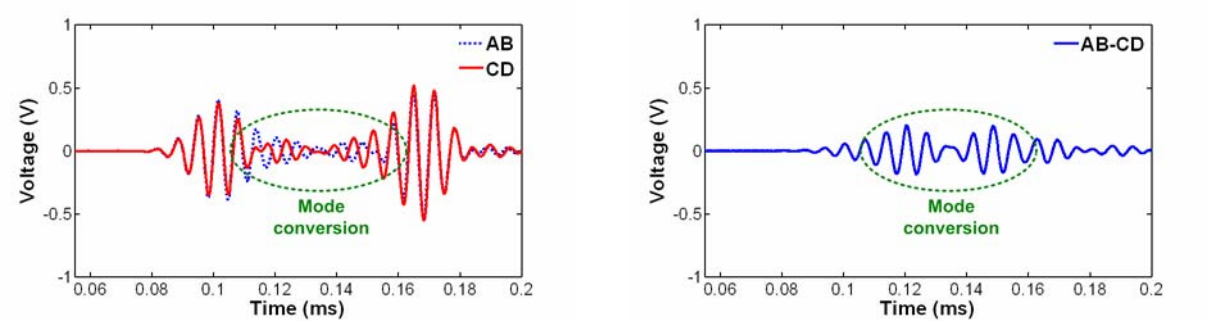

(a) Signals AB and CD with a 3 mm notch (b) Difference between signals AB and CD

Figure 12. Comparison of signals AB and CD with a 3 mm depth notch

3.2. Instantaneous damage diagnosis

In the previous section, it has been shown that damage-sensitive features can be identified from instantaneously measured Lamb wave signals. However, a statistical damage diagnosis is still required to differentiate signals due to damage from error signals produced by variations in PZT size, alignment, and bonding condition. In this section, attention has been paid to determining decision boundaries for damage diagnosis without relying on previously established thresholds.

3.2.1. Damage classification using instantaneously measured Lamb wave signals

Signals AB and CD are indistinguishable when there is no crack as shown in Figure 6. This is based on the assumption that all PZT transducers are identical and PZTs A and D or (PZTs B and C) are perfectly collocated. In practice, these assumptions cannot be fully satisfied because of variations in PZT size, alignment and bonding condition [4]. This imperfection in PZTs may generate initial differences in signals AB and CD even in the absence of crack and lead to positive false alarms.

Here, a damage detection scheme is developed based on the premise that mode conversion produces signal differences between signals AB and CD that are bigger than the initial differences due to PZT imperfection. The proposed technique takes advantage of not only signals AB and CD but also signals AC and BD to extract mode conversion in the presence of variations of the PZT size, alignment and bonding. The uniqueness of the proposed damage classification scheme is that threshold values for damage classification is obtained using only signals instantaneously measured from the current state of the system without relying on predetermined threshold values.

In Figure 13, signal AB is schematically drawn based on the sign definition presented in section 2.2 assuming a notch is closer to PZT A. From Figure 13, it can be shown that signal AB is a simple superposition of signals S_0, MC_1, MC_2 and A_0. Signal S_0 indicates a time signal that contains only the S_0 mode but its length is identical to that of signal AB. Signal MC_1, signal MC_2 and signal A_0 are defined in a similar fashion. MC_1 and MC_2 represent the first and second arrivals of Lamb wave modes created by mode conversion, respectively. Note that MC_1 and MC_2 could be either S_0/A_0 or A_0/S_0 modes depending on the relative position of crack and the actuating and sensing PZTs used for the signal measurement. For instance, MC_1 denotes a S_0/A_0 mode in signal AB when a notch is closer to PZT A than PZT B. This is because the S_0/A_0 mode arrives at PZT B earlier than the A_0/S_0 mode. Similarly, signal MC_2 in signal AB represents the A_0/S_0 mode.

Similar to signal AB, signals AC, BD, and CD can be also expressed as combinations of individual Lamb wave signals [Figure 14]. In Figure 14, these four signals are schematically shown emphasizing the relative phases of individual Lamb modes among these signals. For instance, the S_0 and MC_1 modes in signal AC are out-of-phase compared to these modes in signal AB. Therefore, signal AC can be obtained by flipping signals S_0 and MC_1 and summing up signals S_0, MC_1, MC_2 and A_0 all together. Signals BD and CD are related to signals S_0, MC_1, MC_2 and A_0 in similar manners. Based on these observations, the relationship between the signals that can be measured (signals AB, AC, BD and CD) and the individual Lamb signals (signals S_0, MC_1, MC_2 and A_0) can be obtained as follows:

$$\begin{bmatrix} \text{Signal AB} + e_{AB} \\ \text{Signal AC} + e_{AC} \\ \text{Signal DB} + e_{DB} \\ \text{Signal DC} + e_{DC} \end{bmatrix} = \begin{bmatrix} 1 & 1 & 1 & 1 \\ 1 & 1 & -1 & -1 \\ 1 & -1 & 1 & -1 \\ 1 & -1 & -1 & 1 \end{bmatrix} \begin{bmatrix} \text{Signal } S_0 + e_{S0} \\ \text{Signal } MC_1 + e_{MC1} \\ \text{Signal } MC_2 + e_{MC2} \\ \text{Signal } A_0 + e_{A0} \end{bmatrix} \quad (1)$$

Because of measurement errors and variations in PZT size, alignment and bonding condition, error terms are added in Equation (1). Here, e_{AB} is an error signal in the measured signal AB that is superimposed to the exact signal AB, and e_{AC}, e_{BD}, and e_{CD} are defined similarly. e_{S0}, e_{MC1}, e_{MC2} and e_{A0} represent error signals in each decomposed Lamb mode signals. While Equation (1) illustrates how different combinations of individual Lamb mode signals constitute each measurable signal, Equation (2) below shows how each individual mode signal can be extracted from the measured signals AB, AC, BD and CD. For instance, signal S_0 can be extracted by adding signals AB and CD and subtracting signals AC and BD. Similarly, signal MC_1 can be isolated by adding signals AB and BD and subtracting signals AC and CD.

$$\begin{bmatrix} \text{Signal } S_0 + e_{S0} \\ \text{Signal } MC_1 + e_{MC1} \\ \text{Signal } MC_2 + e_{MC2} \\ \text{Signal } A_0 + e_{A0} \end{bmatrix} = \frac{1}{4} \begin{bmatrix} 1 & 1 & 1 & 1 \\ 1 & 1 & -1 & -1 \\ 1 & -1 & 1 & -1 \\ 1 & -1 & -1 & 1 \end{bmatrix} \begin{bmatrix} \text{Signal AB} + e_{AB} \\ \text{Signal AC} + e_{AC} \\ \text{Signal DB} + e_{DB} \\ \text{Signal DC} + e_{DC} \end{bmatrix} \quad (2)$$

So far, it has been assumed that a notch is located closer to PZT A than PZT B if it exists. In reality, the location of the notch is unknown in advance. When the notch is formed closer to PZT B, the MC_1 and MC_2 modes in signals MC_1 and MC_2 are switched. That is, the MC_2 mode appears in the estimated signal MC_1 instead of the estimated signal MC_2. (Note that the definition of the MC_2 mode is the second arrival of the converted mode, and it appears in the A_0 region of signal MC_1.) From these observations, it is found that Equation (2) can be still used regardless of the location of the notch. In fact, it can be used to decide whether the notch is closer to PZT A or B. For example, if a mode found in signal MC_1 is located in the S_0 region, the notch is located closer to PZT A. Conversely, if the MC_2 mode is found in the A_0 region of signal MC_1 instead of the S_0 region, it confirms that the notch is closer to PZT B. Therefore, once the existence of mode conversion is determined, the location of the defect can be also determined by checking the location of the mode in signal MC_1.

According to Equation (2), the measured signals can be separated into individual Lamb mode signals S_0, MC_1, MC_2 and A_0. Note that only signals MC_1 and MC_2 contain Lamb modes created by damage (MC_1 and MC_2, respectively). Ideally, signals MC_1 and MC_2 should be zeros in the absence of damage. In practice, however, due to e_{MC1} and e_{MC2} that are superimposed to the exact signals MC_1 and MC_2, signals MC_1 and MC_2 may not be zeros even without damage. Since e_{MC1} and e_{MC2} cannot be extracted from signals MC_1 and MC_2 using Equation (2) only, it is challenging to determine whether additional modes in these signals are due to mode conversion or PZT imperfections. To tackle this issue, a new damage classifier is developed to determine if the non- zero responses in signals MC_1 and MC_2 are due to mode conversion or simply due to initial errors.

The damage identification scheme proposed in this study starts from the decomposition of individual Lamb mode signals from measured signals using Equation (2). Next, the maximum absolute amplitude of the error components, e_{S0} and e_{A0}, in signals S_0 and A_0 are estimated. Because the arrival time of the S_0 mode in signal S_0 is known, the non-zero response of signal S_0 outside the S_0 mode is mainly attributed to e_{S0}. Therefore, the maximum amplitude of e_{S0} can be estimated from the rest of signal S_0 where the S_0 mode does not exist. The maximum absolute amplitude of e_{A0} can be also estimated from signal A_0 in a similar fashion. Then, the threshold value for damage classification is set to be the maximum absolute amplitude of e_{S0} and e_{A0}. Finally, the existence of damage is determined by comparing the amplitudes of signals MC_1 and MC_2 with respect to the threshold value. In this way, a crack can be detected if the crack produces signal differences between signals AB and CD that are bigger than the initial differences due to PZT imperfection and measurement errors. Note again that no predetermined

threshold values are required during this damage classification procedure because the threshold value is obtained from instantaneously measured signals AB, AC, BD, and CD. The applicability of the proposed thresholding technique is experimentally investigated in the following subsection.

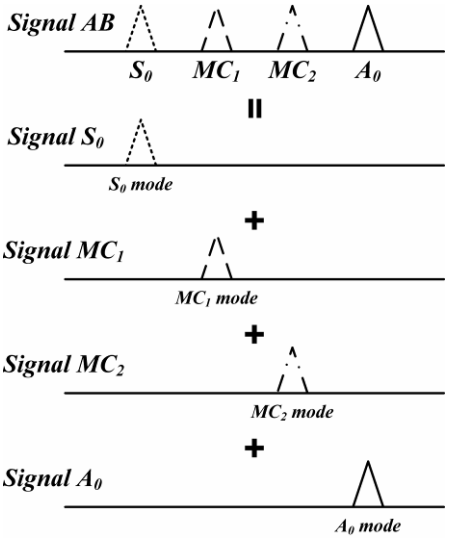

Figure 13. Decomposition of signal AB into individual Lamb wave mode signals (When a notch is closer to PZT A)

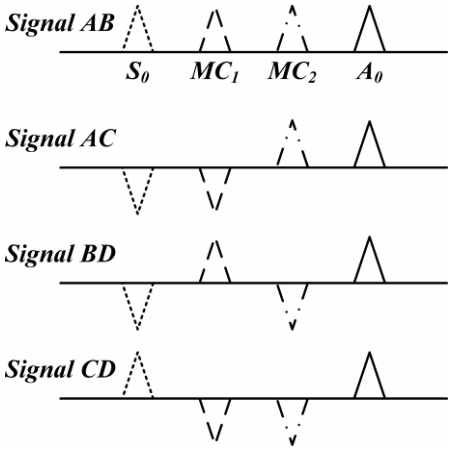

Figure 14. Comparison of relative phase information among signals AB, AC, BD and CD (When a notch is closer to PZT A)

3.2.2. Damage diagnosis using experimentally obtained Lamb wave signals

To explain the proposed damage diagnosis technique, Lamb wave signals measured using the setup in 3.1.2 were used. First, each Lamb mode signal is estimated from signals AB, AC, BD and CD measured from an unknown condition of the specimen. Figure 15 displays individual Lamb mode signals decomposed using Equation (2). In Figure 15 (a), the estimated signal S_0 is shown as a superposition of the exact signal S_0 and the error signal, e_{S0}. Similarly, signal A_0 shown in Figure 15(b) illustrates that the error signal e_{A0} is superimposed to the exact signal A_0. Signals MC_1 and MC_2 are also drawn in Figure 15 (c) and Figure 15 (d). Ideally, signals MC_1 and MC_2 should be zero for the entire length of the signals in the absence of damage. However, due to PZT imperfections, additional modes appeared in signals MC_1 and MC_2.

Once the individual Lamb mode signals are decomposed, the threshold for damage classification is set to be the maximum absolute amplitude of error components, e_{S0} and e_{A0}, in signals S_0 and A_0. The estimated signal S_0 is composed of the exact signal S_0 and e_{S0} as shown in Figure 15. Furthermore, it can be shown that the S_0 mode exists only in a certain portion of the estimated signal S_0 while e_{S0} is present for the entire length of the estimated signal S_0. Therefore, the maximum absolute amplitude of e_{S0} can be estimated from a portion of the estimated signal S_0 where the S_0 mode does not exist. To accomplish this, the estimated signal S_0 is divided into two regions, S_0 and A_0 regions, as shown in Figure 15. Here, the boundary between two regions is placed exactly in the middle of the S_0 and A_0 modes. Because the S_0 mode always exists only in the S_0 region, the response in the A_0 region is attributed only to e_{S0}. Therefore, the maximum absolute amplitude of e_{S0} is estimated from the A_0 region as shown in Figure 15 (a). In a similar manner, the maximum absolute amplitude of e_{A0} is estimated from the S_0 region of the estimated signals A_0 as depicted in Figure 15 (b).

From the estimated maximum absolute amplitude of e_{S0} and e_{A0}, the upper and lower limits for damage diagnosis are established as shown in Figure 16 (a). It is assumed that, if the amplitudes of MC_1 and MC_2 modes exceed one of the threshold values, the mode conversion beyond PZT imperfections or measurement noises is induced by the notch. Note that these threshold values for damage classification are strictly estimated from signals AB, AC, BD and CD instantaneously measured from the system's current state. That is, the dependence on the prior baseline data is eliminated during the damage classification process.

In Figure 16 (a), the proposed diagnosis scheme is applied to the signals obtained from the pristine condition of the specimen. Figure 16 (a) illustrates that both MC_1 and MC_2 modes in the S_0 and A_0 regions did not exceed the threshold values determined from e_{S0} and e_{A0}. Therefore, it can be concluded that these signals are obtained from the undamaged condition of the test article.

Next, the proposed scheme was applied to the signals measured from the 3 mm notch case. Four decomposed signals using Equation (2) are drawn in Figure 15 along with the signals obtained from the undamaged case for comparison. Figure 15 (a) and Figure 15 (b) showed that the occurrence of damage changed signals S_0 and A_0 very little. Furthermore, it is revealed that the amplitudes and shape of e_{S0} and e_{A0} did not change much because they were not related to mode conversion. On the other hand, the appearance of mode conversion is clearly observed in signals MC_1 and MC_2 [Figure 15 (c) and Figure 15 (d)]. After the threshold values are determined from the maximum absolute amplitude of e_{S0} and e_{A0}, it is tested whether the MC_1 mode in the S_0 region of signal MC_1 and the MC_2 mode in the A_0 region of signal MC_2 exceed the thresholds. Figure 16 (b) shows that both MC_1 and MC_2 modes in signals MC_1 and MC_2 exceeded the threshold values determined from the damaged condition of the structure. Therefore, these signals are classified to be damaged.

In this section, a new damage classifier that does not rely on predefined threshold values has been introduced. The classifier was developed based on the decomposition technique introduced in 3.2.1. The advantage of the decomposition technique is that only converted modes can be extracted from measured Lamb wave signals. In the following parts of this report, this decomposition technique plays important roles for damage identification.

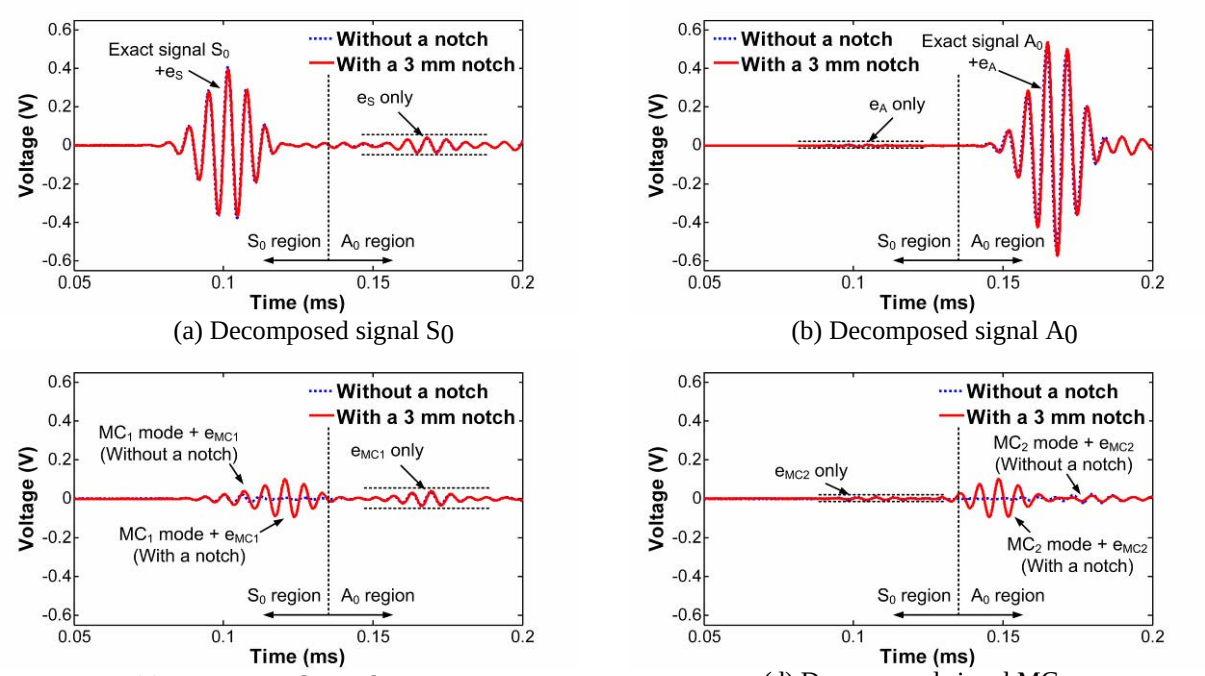

(a) Decomposed signal S_0

(b) Decomposed signal A_0

(c) Decomposed signal MC_1

(d) Decomposed signal MC_2

Figure 15. Decomposition of individual Lamb mode signals S_0, MC1, MC2 and A_0 from measured signals AB, AC, BD and CD using Equation (2)

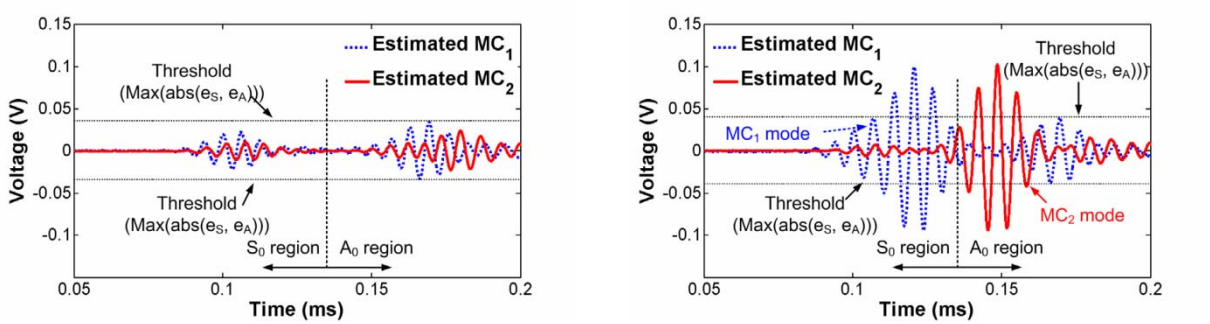

(a) Comparison of the amplitudes of estimated MC_1 and MC_2 with instantaneously obtained threshold values (without damage)

(b) Comparison of the amplitudes of estimated MC_1 and MC_2 with instantaneously obtained threshold values (with a 3 mm notch)

Figure 16. Autonomous damage identification using instantaneously obtained threshold values instead of predetermined decision boundaries (Max(abs(e_{S0} , e_{A0})) denotes maximum absolute value of e_{S0} and e_{A0}.

3.3. Environmental and operational variations

In this project, the effect of environmental and operational variations on the proposed technique has been investigated. Especially, experiments were conducted in the controlled laboratory to validate the robustness of the proposed NDT technique to varying temperature conditions.

3.3.1. Experimental setup for varying temperature tests

For this study, an aluminum plate of 455 mm×254 mm×3 mm was used as shown in Figure 17. The size of the plate was mainly limited by the available space of the temperature chamber used later for temperature experiments. The Young's modulus of this T6 aluminum plate was 310 MPa.

Circular PZTs (6.35 mm in diameter and 0.25 mm in thickness) were purchased from American Piezo Ltd. They had a Curie temperature of 360^0C and the maximum operational temperature of 180 ^{0}C. The d_{33} piezoelectric charge constant, the capacitance value and the Young's Modulus were 4×10^{-10} m/V, 1.50 nF, 6×10^{10} N/m^2, respectively. PZTs A and D were collocated and attached on the other side of the plate, and PZTs B and C were mounted in a similar fashion. The PZTs were attached so that their poling directions were identical to the configuration shown in Figure 17. (In the figure, the positive poling direction of individual PZT is shown with an arrow.) PZTs A and B (or PZTs C and D) were 215 mm apart each other.

For the attachment of PZTs to the specimen, M-bond 200cyanoacrylate adhesive from Vishay measurements group was used. Based on the manufacturer's specification, this M-bond adhesives could be used for a one-cycle proof test over 90 ^{0}C or -185 ^{0}C. But, the normal operating temperature range was -30 ^{0}C to 65 ^{0}C. To secure the wires to the specimen, high temperature Teflon tapes from 3M Corporation (3M Scotch Brand 5412) were used. In addition, high temperature wires were used.

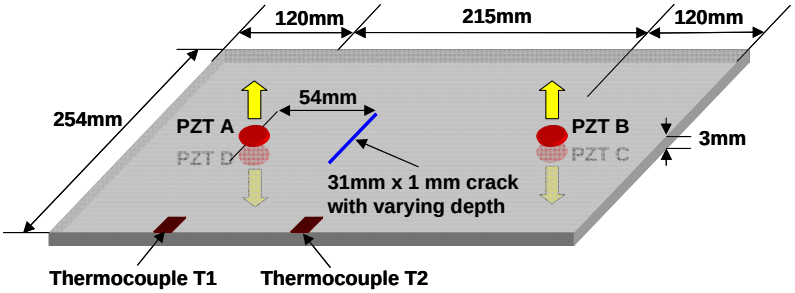

Figure 17. Dimension and configuration of the aluminum test specimen with a uniform thickness: The arrows denote the positive polarization directions of each PZTs.

The data acquisition system used in this study is shown in Figure 18. The data acquisition system was composed of a laptop computer, an arbitrary waveform generator (AWG), a high-speed signal digitizer (DIG), a low noise preamplifier (LNP) and a multiplexer. Using the 14-bit AWG, a toneburst signal with a 10 peak-to-peak voltage and a driving frequency of 280kHz was generated and applied. First, PZT A shown in Figure 17 was excited by this input waveform. Then, PZT A generated elastic waves and the response was measured at PZT B. When the waves arrived at PZT B, the voltage output from PZT B was filtered and amplified by the LNP with a gain of ten and measured by the DIG. The sampling rate and resolution of the DIG were 20 MS/sec and 16 bits, respectively. In order to improve the signal-to-noise ratio, the forwarding signals were measured ten times and averaged in the time domain. After the forwarding signals from PZT A to PZT B (signal AB) were measured, the same process was repeated by measuring signals AC, DB and DC. The entire experimental process without averaging took less than 1 minute. By increasing the number of channels, it is expected that the data collection time can be further shortened. The switching of the exciting and sensing PZTs was accomplished using the multiplexer and controlled by the LabVIEW software installed on the laptop computer. Initial data was collected without any crack in the specimen, and then a crack was introduced between PZTs A and B, 54 mm from PZT A as shown in Figure 19. The length and width of the crack was 31 mm and 1 mm, respectively, and the crack depth was increased from 0 mm to 0.5 mm, 1.0 mm and 2.0 mm.

As shown in Figure 17, two thermocouples T1 and T2 are instrumented at the middle and quadrant points of the specimen. The thermocouples were connected to BK Precision 725 Humidity and Temperature Meter. As part of temperature experiments shown in Figure 20(a), an infrared heater from Protherm Heater (model #12014) was used to simulate partial head-up of the specimen. For the experimental results provided in the following subsection, the reading from thermocouple T2 was reported.

Another temperature experiment was conducted using a MicroClimate temperature/humidity chamber. The chamber is designed to operate in a temperature range of -73ºC to 190ºC and a maximum relative humidity of 95%. In this study, only the temperature value was controlled.

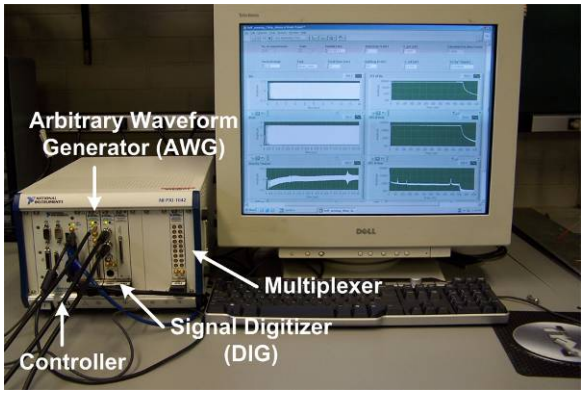

Figure 18. A data acquisition system

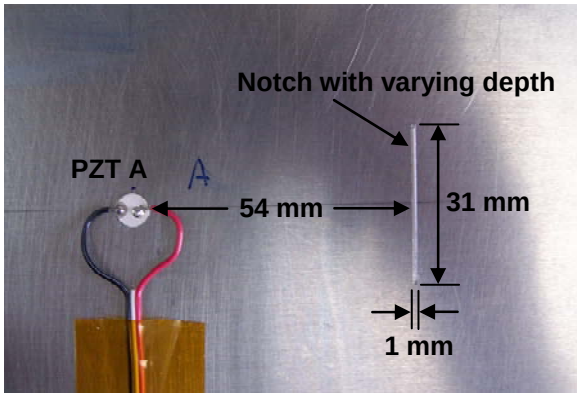

Figure 19. A notch with an increasing depth

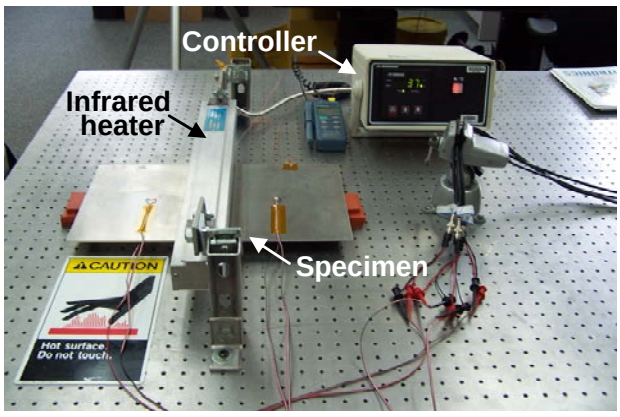

(a) A inferred heater (b) A temperature chamber

Figure 20. Two experimental setups for temperature variations

3.3.2. Crack detection under varying temperatures

During the experiments, multiple Lamb wave signals are measured from the aluminum plate in both intact and damaged conditions under varying temperatures. Since the size of the plate was not large enough to avoid reflective Lamb wave modes from the boundary, the damage classifier proposed in section 3.2 could not be used in this specific case. Note that the error signals, which the former classifier utilized, were superimposed by the reflections in this case. Therefore, a new thresholding technique (Technique 2) was proposed in this subsection.

Technique 2 starts by decomposing measured signals AB, AC, DB and DC into signals S_0, MC_1, MC_2 and A_0 again. Then, the standard deviation of signal MC_1, σ_{MC1} is computed. If there is no defect, the variance of signal MC_1 is mainly attributed to the initial errors. Assuming that the initial errors have a normal distribution of zero mean and σ_{MC1} standard deviation, 99.7% of the data points in signal MC_1 should be within the range of $-3\sigma_{MC1}$ to $3\sigma_{MC1}$. Once actual mode conversion appears in signal MC_1, the maximum absolute amplitude of the actual MC_1 mode should go outside this range. Therefore, the existence of a crack can be identified when $\max(MC_1)$ becomes larger than σ_{MC1}. In a similar fashion, the threshold for signal MC_2 can be set to be σ_{MC2}.

$$\text{If } \max(|MC_1|) > 3\sigma_{MC1} \text{ and } \max(|MC_2|) > 3\sigma_{MC2}, \text{ a crack exists} \quad (3)$$

The next step was to examine if the proposed NDT technique and damage classifier are robust even under changing temperature conditions. The variations of measured time signals and decoupled Lamb modes with respect to temperature were illustrated in Figure 21 using representative signals. These signals were obtained when the specimen with 2mm deep crack was placed inside the temperature chamber. The amplitude increase and phase delay of the signals were observed as the temperature increased from -30 ºC to 70 ºC. It should be noted that because the temperature variation itself could cause significant changes in the measured signal's amplitude and phase, it would be challenging to perform pattern comparison with the baseline signals for the purpose of damage diagnosis.

All damage diagnosis results from varying temperature conditions are summarized in Table 2. In the first 4 rows (cases 1-4), false-positive studies were conducted using the intact specimen. For all cases examined, there were no indications of false alarms. For cases 1 to 4, the temperature was controlled using the infrared heater from 22 ºC to 55 ºC. Note that the temperature reported here was obtained from thermocouple T2 shown in Figure 17, and thermocouple T1 was used as the set point for the temperature controller. Because the infrared device locally heated up the middle portion of the specimen, a large temperature gradient between the center and the edge of the specimen was observed. For instance, the reading form T2 was close to 100 ºC for case 4 in Table 2, while T1 was about 50 ºC. Note that a broader spectrum of temperature variations was not examined using the intact specimen to avoid any potential damage to the PZT transducers before performing subsequent damage cases. For cases 5 to 16 in Table 2, the specimen with 1 mm crack was subjected to temperature increase from 5ºC to 60ºC using either the infrared heater or the temperature chamber. For all cases investigated, the maximum absolute amplitudes of the MC_1 and MC_2 modes exceeded the threshold values obtained from Technique 2. Furthermore, the numbers of outliers for each threshold values remained reasonably consistent. For the remaining cases, (cases 17 – 27), the specimen with 2 mm-deep crack was subjected a broad temperature variation of -30ºC to 70 ºC using the temperature chamber. Compared to cases 5 to 17, larger numbers of outliers were observed for cases 17 to 27.

It was concluded that a crack deeper than 1 mm was detectable when the 3 mm specimen was investigated in the temperature range of -30 ºC to 70 ºC as long as there was no degradation of the PZTs' piezoelectricity and bonding conditions. The applicability of the proposed technique was demonstrated under the limited conditions: The consistent bonding of the PZTs and the precise alignment of the collocated PZTs were critical to the success of the proposed technique. In addition, the current technique is only applicable to structures with uniform thickness. As long as mode conversions reflected or refracted from the crack are measurable by one of the PZTs, the mode conversion due to the crack formation should be detected in theory. However, the effects of the crack location and orientation were not investigated in this study. Ongoing research is underway to address these issues.

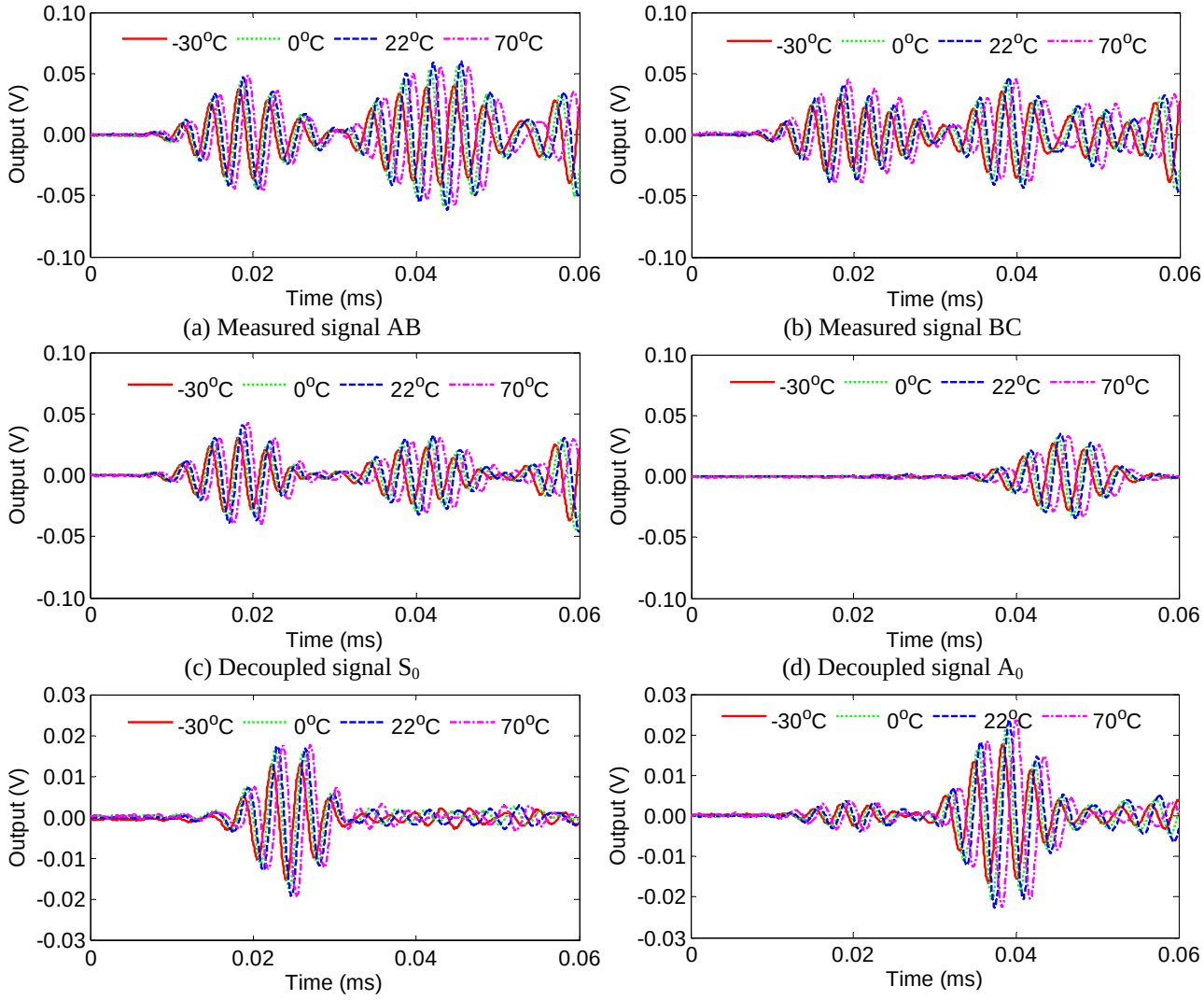

(a) Measured signal AB (b) Measured signal BC

(c) Decoupled signal S_0 (d) Decoupled signal A_0

(e) Decoupled signal MC_1 (S_0/A_0) (f) Decoupled signal MC_2 (A_0/S_0)

Figure21. Variation of measured time signals and decomposed modes with repect to temperature (with 2 mm deep crack : -30°C 0°C 22°C 70°C)

Table 2: Number of outliers outside the threshold values (under changing temperatures)

Crack depth	#	T2 (°C)*	Technique 2		Temp. Control	Date (mm/dd/yy)
			S_0/A_0	A_0/S_0		
0 mm	1	22	0	0	Infrared heater	08/01/07
	2	39	0	0		08/01/07
	3	40	0	0		08/01/07
	4	55	0	0		08/01/07
1 mm	5	23	47	31	Infrared heater	08/07/07
	6	30	44	39		08/07/07
	7	40	44	39		08/07/07
	8	51	44	39		08/07/07
	9	05	43	32	Temp. chamber	08/07/07
	10	10	45	28		08/08/07
	11	15	44	31		08/08/07
	12	21	45	31		08/09/07

	13	23	44	31		08/08/07
	14	41	45	37		08/09/07
	15	50	42	36		08/09/07
	16	60	42	40		08/09/07
2 mm	17	-30	43	41	Temp. chamber	08/13/07
	18	-20	46	43		08/13/07
	19	-10	45	41		08/13/07
	20	-5	49	49		08/13/07
	21	0	47	39		08/13/07
	22	11	48	43		08/13/07
	23	17	47	41		08/13/07
	24	22	46	46		08/13/07
	25	50	47	47		08/13/07
	26	60	51	55		08/13/07
	27	70	50	51		08/13/07

*The temperature reported here was obtained from thermocouple T2 shown in Figure 17.

3.4. Extension to more complex structures

So far, the proposed technique has been tested for simple plates although many civil infrastructures have more complex structural features such as holes and stiffeners. In this project, not only the effect of through-the-thickness holes but also stiffeners on the proposed technique is investigated.

3.4.1. Understanding the effect of through-the-thickness holes

An array of holes creates multiple reflections and refractions of Lamb waves, and these multiple reflections and refractions may cause difficulties in analyzing responses of Lamb waves [5]. Because a symmetric configuration of waveguide thickness variation is preserved even in the existence of through-the-thickness holes, the holes do not produce mode conversion [2]. Therefore, it is expected that those holes do not affect the performance of the proposed technique. This theoretical expectation was validated from numerical simulations and experiments.

Since the through-the-thickness hole could not be modeled under plain strain assumption, Lamb wave propagation in a three-dimensional aluminum plate was simulated using PZFlex 1.4. The configuration of specimen including a hole, a notch and PZT wafer transducers are shown in Figure 22.

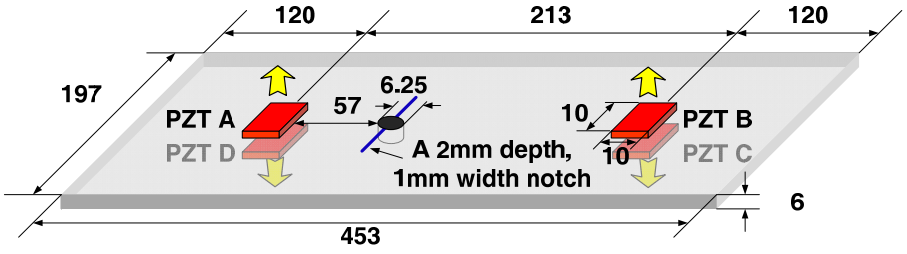

Figure 22. Configuration of the specimen with collocated PZTs, a notch and a through-the-thickness hole for numerical simulation (all dimension in mm). The arrows indicate the positive poling direction of PZTs

In Figure 23, simulation results are illustrated. As expected, even in the presence of the through-the-thickness hole, simulated signals AB and DC (or signals AC and DB) were identical because the hole was not the source of mode conversion [Figure 23 (a) and Figure 23 (b)]. Signals AB and DC (or signals AC and DB) became different after the notch was formed [Figure 23 (c) and Figure 23 (d)]. These results are similar to the simple plate case.

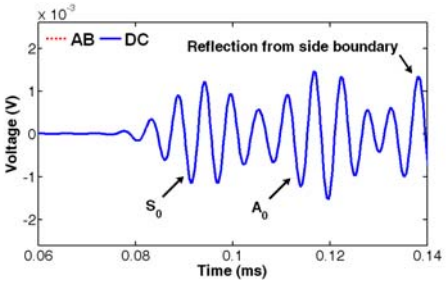

(a) Signals AB and DC with only a hole

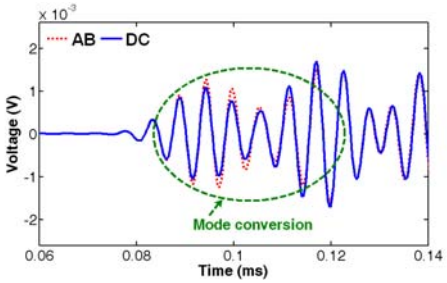

(b) Signals AB and DC with a hole and a notch

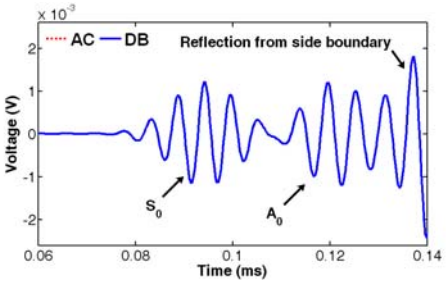

(c) Signals AC and DB with only a hole

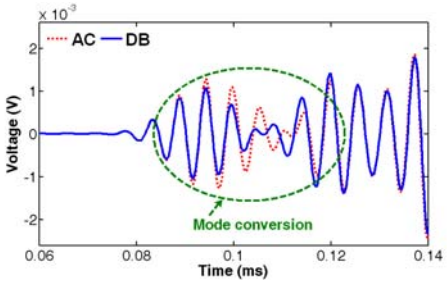

(d) Signals AC and DB with a hole and a notch

Figure 23. Comparison of simulated signals AB and DC (or signals AC and DB)

After S_0, A_0, MC_1 and MC_2 were decoupled using Equation (2), it was shown clearly that the through-the-thickness hole did not produce converted modes [Figure 24 (c) and Figure 24 (d)]. Also, the patterns of the S_0, A_0, MC_1, and MC_2 modes did not change much even in the presence of the hole.

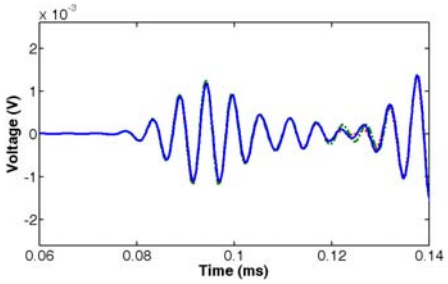

(a) Decomposed S_0 modes

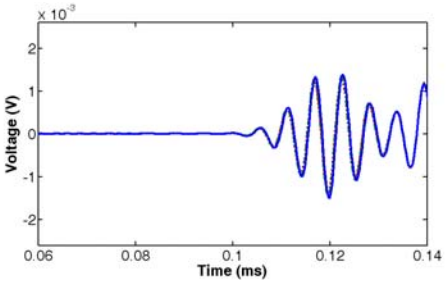

(b) Decomposed A_0 modes

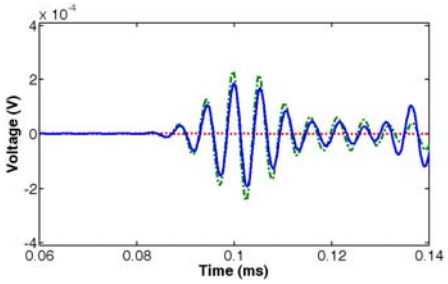

(c) Decomposed MC_1 modes

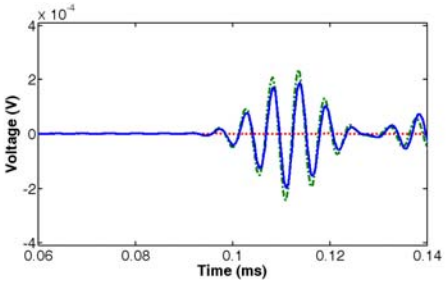

(d) Decomposed MC_2 modes

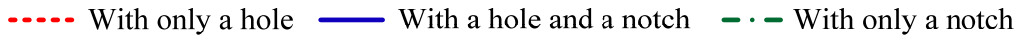

Figure 24. Decomposed signals S_0, MC_1, MC_2 and A_0 from simulated Lamb wave signals using Equation (2), where signal MC_1 and MC_2 represent the first and the second mode conversion, respectively.

After the numerical simulation, the effect of the through-the-thickness holes has been investigated experimentally. The aluminum plate used in this study has identical dimensions with the one in Figure 22. Except for the input frequency (180kHz) and the gain of LNP (50), other parameters were selected to be identical to the values in section 3.1.

First, one hole and the notch were introduced in series and the responses from that specimen were measured [Figure 25]. Next, two additional holes were formed and similar procedure was repeated. The three holes were 50 mm apart to each other. The diameter of the holes and the dimensions of the notch are shown in Figure 25 (b).

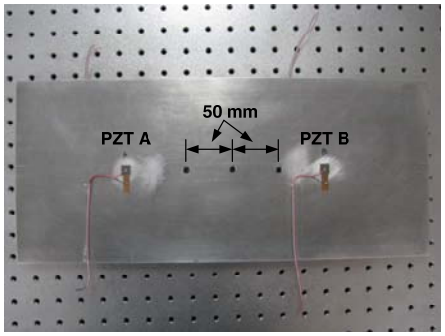

(a) The specimen with collocated PZTs, a notch and through-the-thickness holes for experiments.

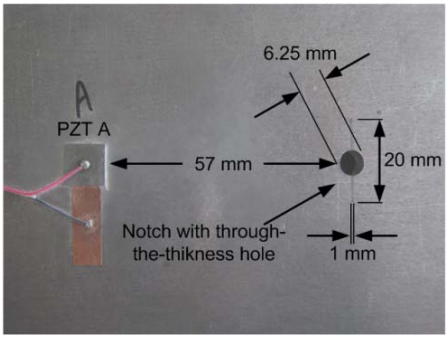

(b) A notch was produced first and then a through-the-thickness hole was introduced

Figure 25. The specimen for experiments to consider the effect of the through-the-thickness holes

Figure 26(a) and Figure 26(b) clearly showed that the shapes and amplitudes of the unconverted modes (S_0/ S_0 and A_0/A_0 modes) were not affected much by either the notch or the holes. Additionally, converted Lamb wave modes due to the notch appeared in signals MC_1 and MC_2 regardless to the number of holes. Also note that, the damage classifier proposed in section 3.2 can be applied to these decomposed signals because the effect of the through-the-thickness holes on the proposed technique is minimal.

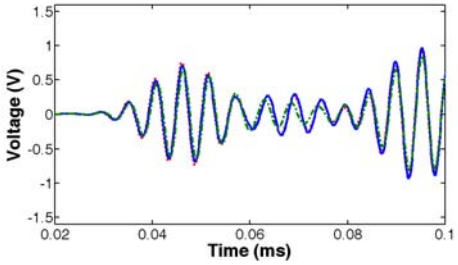

(a) Comparison of signals S_0

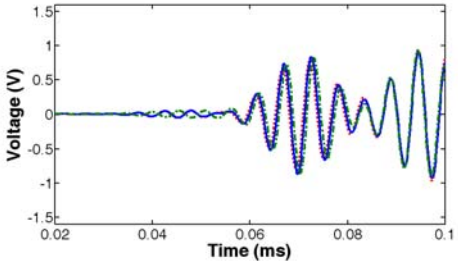

(b) Comparison of signals A_0

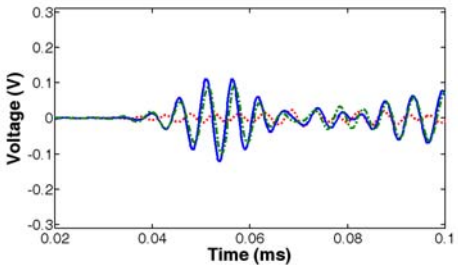

(c) Comparison of signals MC_1

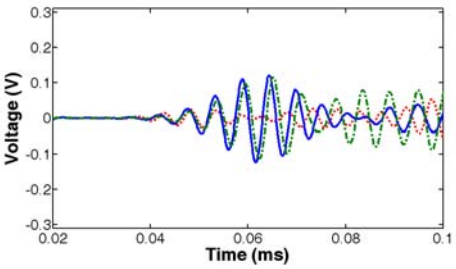

(d) Comparison of signals MC_2

With only a hole — With a hole and a notch — With 3 holes and a notch

Figure 26. Comparison of decomposed signals among the condition of the plate with only a hole, with a hole and a notch and with 3 holes and a notch

3.4.2. Understanding the effect of stiffeners

In this subsection, the proposed damage detection technique is extended to the plate including a stiffener. Since the configuration of waveguide become no longer symmetrical when the stiffener is introduced to the wave path, mode conversion can occur even though damage is not formed. Mode conversion due to the stiffener may cause difficulties in analyzing the Lamb wave signals measured from the structures.

In Figure 27, some of the converted Lamb wave modes due to the stiffener and notch are illustrated. In the plate with a single stiffener, there exist two possible wave paths: (1) the wave propagation only inside the plate [Figure 27 (a)], and (2) the wave path through the stiffener [Figure 27 (b)]. In the first path, a single mode is separated into four individual modes because there are two sources of mode conversion, the stiffer and the notch. (Underline denotes that the mode is produced by the notch.) Therefore, the S_0 and A_0 modes produce total 8 modes in the first path. In the second path, three sources of mode conversion exist. The first and the second mode conversion are occurring when the single mode is entering and propagating out of the stiffer. The third source of mode conversion is the notch. At the end, a single Lamb wave mode is separated into 8 individual modes in the second path. Finally, total 24 Lamb wave modes are measured at the receiving transducer in the presence of the stiffener and the notch.

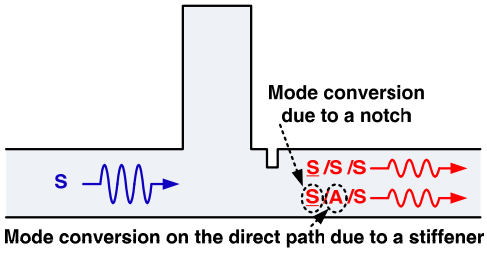

(a) Converted and transmitted Lamb modes due to a stiffener and a notch on the direct path

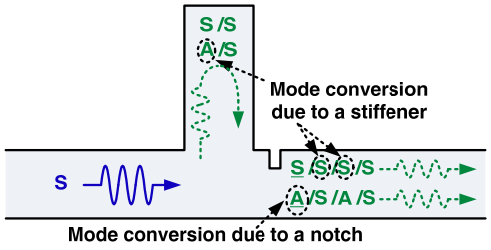

(b) Converted and reflected Lamb modes due to a stiffener and a notch on the path including a stiffener

Figure 27. A scheme of Lamb wave propagation on the plate including a stiffener

The PI is now preparing for a journal paper that includes detailed analysis of each Lamb wave modes in the plate with one stiffener case. The main idea of the journal paper is introduced briefly in this report. From measured Lamb wave signals, signals MC_1 and MC_2 can be decomposed. In the absence of damage, these two signals are identical except that signal MC_1 is shifted compared to signal MC_2. This shifting in two signals is caused when the stiffener is not exactly in the middle between PZTs A and B (or PZTs D and C). Also, using information about group velocities of the S_0 and A_0 modes and the geometry of the structure, the amount of shifting can be estimated. Therefore, the mode conversion produced by only stiffener can be compensated by aligning two signals.

On the other hand, signals MC_1 and MC_2 are different even after the alignment in the presence of the notch. Figure 28 illustrates each mode in two signals. For example, even thought the SSA mode in shifted signal MC_1 and the ASS mode in signal MC_2 have same arrival times, they have different amplitudes and shapes. When signal MC_2 is subtracted from the shifted MC_1, multiple Lamb wave modes will remain. This idea was fully validated by numerical simulations as well as experiments.

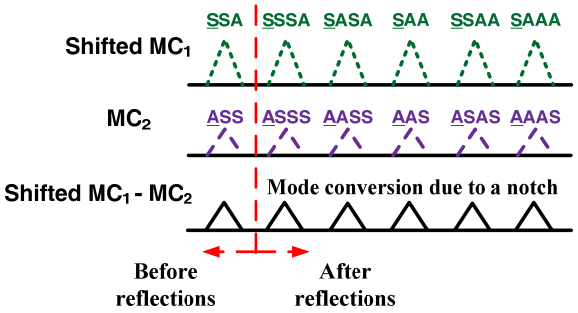

Figure 28. Extracted MC_1 and MC_2 modes of measured signals from the damaged specimen

In Figure 29, the dimensions of the aluminum plate with one stiffener used in this experiment are shown. In the simulation, the plate Figure 29 was modeled as a 2-D structure under plain strain assumption for brevity. COMSOL 3.4 Multiphysics software was used to simulate Lamb wave propagation in a two dimensional aluminum plate with one stiffener. The length of the plate was 70 cm, and its thickness was 6 mm. The depth and the thickness of the stiffener were 90 mm, and 6 mm, respectively. Four identical PZTs with 10 mm length and 0.5 mm thickness were attached to the plate model as shown in Figure 29. The parameters in Table 1 were used in this simulation.

Signals MC_1 and MC_2 decomposed from the Lamb wave signals are shown in Figure 30. Figure 30 (a) and Figure 30 (c) illustrate that the mode conversion due to only the stiffener can be compensated by shifting signal MC_1 in the absence of damage [Figure 30 (e)]. Once a notch of 2 mm depth and 1mm width was introduced right next to the stiffener as is shown in Figure 29, shifted signal MC_1 became different from signal MC_2 as a result of the mode conversion induced by the notch [Figure 30 (d) and Figure 30 (f)].

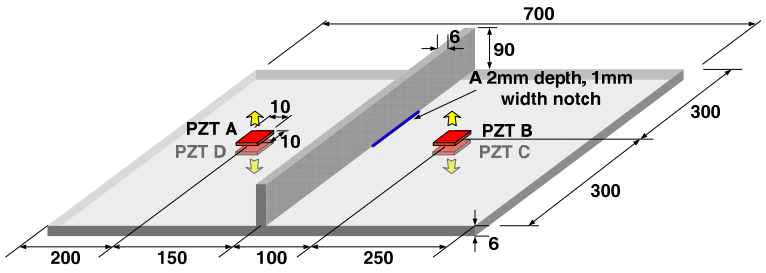

Figure 29. Configuration of the specimen with collocated PZTs, a notch and a stiffener for numerical simulation (all dimension in mm). The arrows indicate the positive poling direction of PZTs

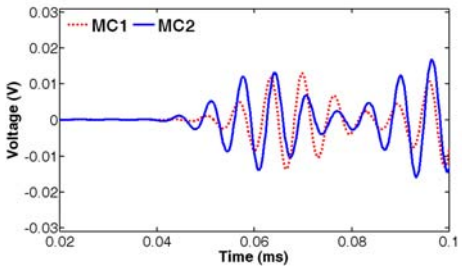

(a) Comparison of signals MC_1 and MC_2 (with only a stiffener)

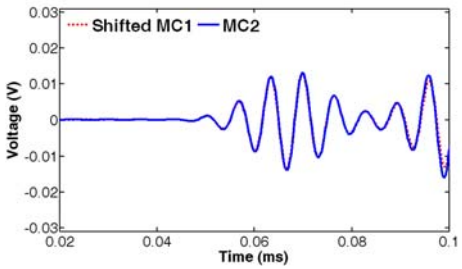

(b) Consideration of the difference of arrival time between signals MC_1 and MC_2 (with only a stiffener)

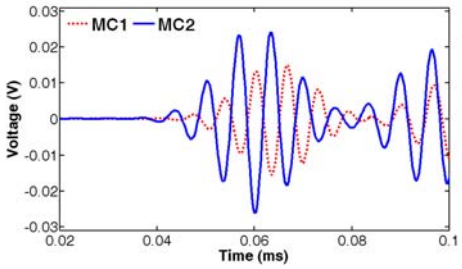

(c) Comparison of signals MC_1 and MC_2 (with a stiffener and a notch)

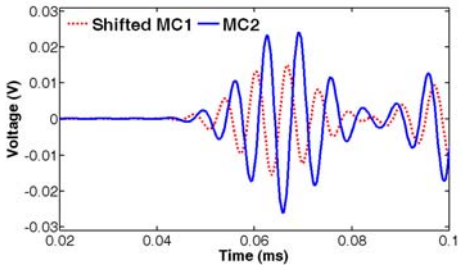

(d) Consideration of the difference of arrival time between signals MC_1 and MC_2 (with a stiffener and a notch)

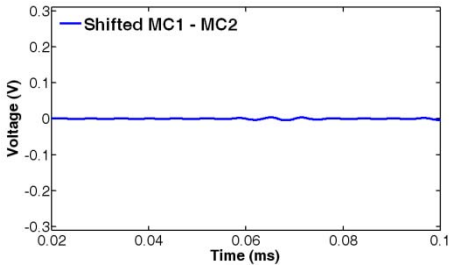

(e) Difference of MC_2 from shifted MC_1 (with only a stiffener)

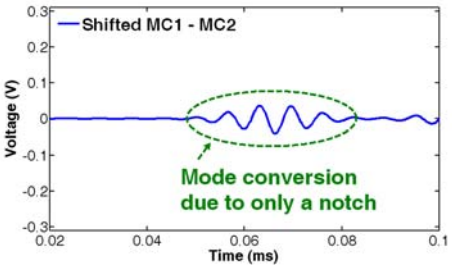

(f) Difference of MC_2 from shifted MC_1 (with a stiffener and a notch)

Figure 30. Comparison of individual Lamb modes and compensation of the difference in the arrival times between MC_1 and MC_2 using simulated Lamb wave signals

After the numerical simulation, the effect of the stiffener has been investigated experimentally. The aluminum plate used in this study has identical dimensions with the one in Figure 29. Except for the gain of LNP (50), other parameters were selected to be identical to the values in section 3.1.

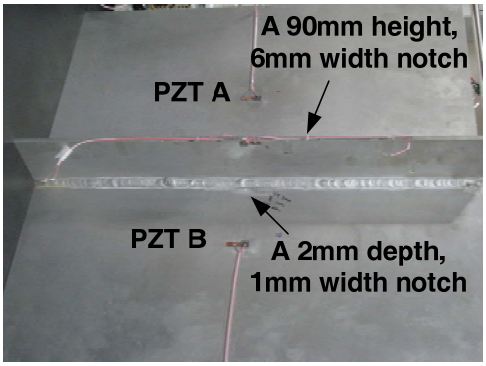

(a) Configuration of a plate including a stiffener and PZTs

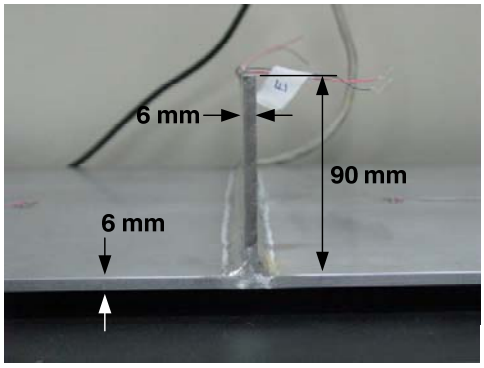

(b) The dimension of a stiffener

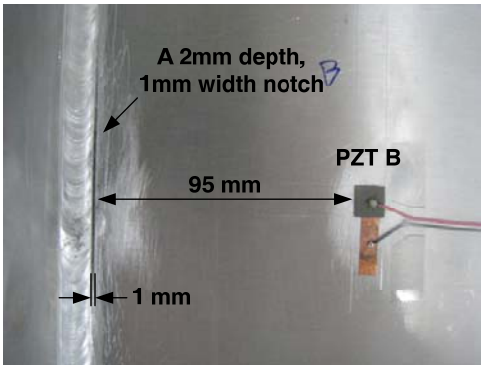

(c) The location and dimension of a notch

Figure 31. Configuration of the specimen

Signals MC_1 and MC_2 decomposed from the measured Lamb wave signals are shown in Figure 32. In the simulation results, signals MC_1 and MC_2 were identical after alignment when the notch was absent. On the other hand, Figure 32(c) showed that the two signals had different amplitudes. It was suspected that the difference in amplitudes was caused by the imperfection in PZT bonding conditions and different welding conditions on both sides of the stiffener. However, signals MC_1 and MC_2 were almost identical in shape. Figure 32(d) showed that signals MC_1 and MC_2 were different in both amplitude and shape due to the presence of the notch. As a part of the project, the damage classifier for this plate with one stiffener case is now being developed and tested.

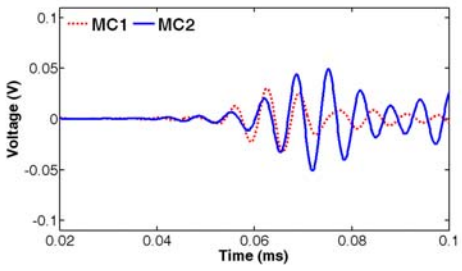

(a) Comparison of signals MC_1 and MC_2 (with only a stiffener)

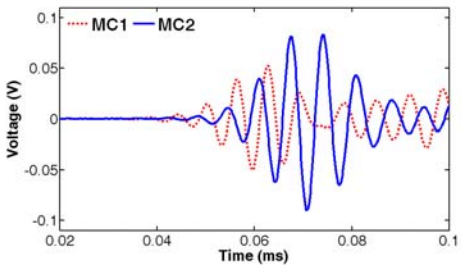

(b) Comparison of signals MC_1 and MC_2 (with a stiffener and a notch)

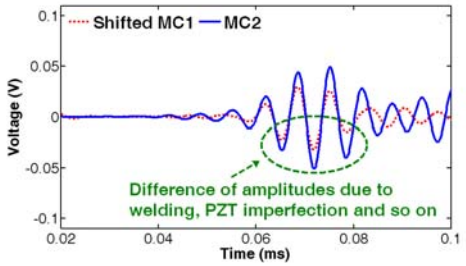

(c) Consideration of the difference of arrival time between signals MC_1 and MC_2 (with only a stiffener)

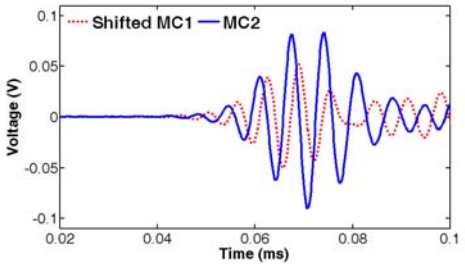

(d) Consideration of the difference of arrival time between signals MC_1 and MC_2 (with a stiffener and a notch)

Figure 32. Comparison of individual Lamb modes and compensation of the difference in the arrival times between MC_1 and MC_2 using measured Lamb wave signals

4. Summary and Conclusion

In this project, the applicability of the proposed NDT technique to crack detection has been fully validated throughout numerical as well as experimental studies. The PI listed the specific objectives of the project below and elaborated on the findings in each objective.

Extraction of Reference-Free Features: In the project, the idea of using PZT polarization characteristics for extracting damage features has been tested numerically and experimentally. The phase information of the measured Lamb wave signals in a time domain depends on whether the sensing PZT is attached to the top or the bottom surface of the plate. Furthermore, the phases of the generated Lamb waves change in accordance with the poling direction of the exciting PZT transducers. Therefore, by controlling the poling directions of the exciting and sensing PZT transducers, it is possible to collect different Lamb wave signals in a wave path. In this project, the use of four collocated PZT transducers was proposed to measure multiple Lamb wave signals. When propagating Lamb waves experienced mode conversion in the presence of damage, only the converted modes due to the damage could be successfully extracted from the Lamb wave signals measured using the PZT transducers.

Instantaneous Damage Diagnosis: Once damage-sensitive features were identified, a theoretical framework for statistical damage diagnosis was developed to fully automate the decision-making procedure. The proposed damage diagnosis aimed to differentiate signals due to damage from error signals produced by variations in PZT size, alignment, and bonding condition. In this project, it has been shown that the measured Lamb wave signals could be decomposed so that converted modes due to damage could be extracted. The decision boundary was chosen from the error signals extracted only from the measured Lamb wave signals. By comparing the amplitudes of the converted modes with those of error signals, automated decision was made. Note that only instantaneously measured Lamb wave signals were used to identify the current condition of the structure.

Environmental and Operational Variations: Varying temperature tests have been conducted in the controlled laboratory. Four PZT transducer wafers were attached to an aluminum plate, and converted modes due to damage were extracted from measured Lamb wave signals. As long as the PZTs' piezoelectricity and bonding conditions were preserved, the crack damage was detectable in the temperature range of -30 ºC to 70 ºC.

Extension to More Complex Structures: Once the basic concept of the reference-free NDT technique was established, it has been extended for more complex structures such as a plate with holes and a plate with one stiffener. Since the through-the-thickness holes were not the sources of mode conversion, the proposed technique could be successfully applied to the plate with multiple holes. As for the plate with one stiffener, it has been shown that mode conversion regardless to the damage could be compensated so that only the converted modes due to the damage could be identified using the proposed technique.

5. References

[1] Viktorov I 1967 *Rayleigh and Lamb Waves* (New York: Plenum Press)
[2] Cho Y 2000 Estimation of Ultrasonic Guided Wave Mode Conversion in a Plate with Thickness Variation *IEEE transactions on ultrasonics, ferroelectrics, and frequency control* 47 591-603
[3] Park H W, Kim S B and Sohn H 2008 Understanding a Time Reversal Process in Lamb Wave Propagation: Theory *Submitted to Wave Motion*
[4] Kim S B, Park H W and Sohn H 2007 Understanding a Time Reversal Process in Lamb Wave Propagations: Experimental Results, *Submitted to Journal of Sound and Vibration*
[5] Fromme P and B S Mahir 2002 Measurement of the scattering of a Lamb wave by a through hole in a plate *Journal of the Acoustical Society of America* 111 1165-1170